Commun. Comput. Phys.
doi: 10.4208/cicp.110509.271009a

Vol. **8**, No. 2, pp. 403-426
August 2010

Optimal Error Estimation of the Modified Ghost Fluid Method

Liang Xu and Tiegang Liu*

LMIB and School of Mathematics and Systems Science, Beijing University of Aeronautics and Astronautics, Beijing 100191, China.

Received 11 May 2009; Accepted (in revised version) 27 October 2009

Available online 12 March 2010

Abstract. The modified ghost fluid method (MGFM) has been shown to be robust and efficient when being applied to multi-medium compressible flows. In this paper, we rigorously analyze the optimal error estimation of the MGFM when it is applied to the multi-fluid Riemann problem. By analyzing the properties of the MGFM and the approximate Riemann problem solver (ARPS), we show that the interfacial status provided by the MGFM can achieve "third-order accuracy" in the sense of comparing to the exact solution of the Riemann problem, regardless of the solution type. In addition, our analysis further reveals that the ARPS based on a doubled shock structure in the MGFM is suitable for almost any conditions for predicting the interfacial status, and that the "natural" approach of "third-order accuracy" is practically less useful. Various examples are presented to validate the conclusions made.

AMS subject classifications: 35L45, 65C20, 76T10

Key words: Modified ghost fluid method, Riemann problem, approximate Riemann problem solver.

1 Introduction

In recent years, with the continuous improvement of numerical simulation and the matureness of various algorithms, many complex flow issues, which were not able to be explored in depth in the past, have reentered the horizons of scientific researchers. Some high resolution schemes for compressible flows, such as the total variation diminishing (TVD) schemes [1, 2] and the essentially non-oscillatory (ENO) schemes [3–5], can work very successfully for pure medium compressible flows. However, when we employ such schemes to simulate multi-medium compressible flows, unexpected difficulties occur due

*Corresponding author. *Email addresses:* xuliang@smss.buaa.edu.cn (L. Xu), liutg@buaa.edu.cn (T. Liu)

to nonphysical oscillations generated in the vicinities of the material interfaces. To suppress the oscillations, various techniques have been developed, see, e.g., [6–9, 11–16, 19].

Among the above mentioned methods, the ghost fluid method (GFM) [11] and other GFM-based techniques [8, 9, 12, 19] provide simple and flexible ways for handling multi-medium flows. The easy extension to multi-dimensions and maintenance of a sharp interface are the advantages of the GFM-based techniques. The key point of these GFM-based techniques is to properly define the properties of the ghost fluids, which is also the primary difference among the various versions of the methods. The original GFM [11] uses the local real fluid velocity and pressure to define the corresponding ghost fluid status, and the density of the ghost fluid is obtained via isobaric fixing [10]. It has been shown, however, that such a definition of ghost fluid status is not efficient when applied to gas-water flows [12].

In fact, the pressure or the velocity across the material interface can have a sudden jump when there is a strong wave interacting with the interface. Whether in the original GFM or its later gas-water version [12], the definition of ghost fluid status is not strictly sufficient to take into account the effects of wave interaction and material properties. To overcome such shortcomings, a modified GFM (MGFM) was developed in [8], where a Riemann problem was defined along the normal direction of the interface and solved using approximate Riemann problem solver (ARPS) to predict the interfacial status. The predicted interfacial status was then utilized to define the ghost fluid status. The MGFM has been shown to be robust and less problem related and successfully applied to various gas-gas, gas-water and fluid-structure coupling problems [8, 9, 20–22]. In addition, it has been proved that the interfacial status captured by the MGFM approximates the exact solution to "second-order accuracy" for the gas-gas Riemann problem [18].

However, we find that the above analytical conclusions are not optimal. In this paper, a further analysis is carried out for the MGFM in the absence of vacuum or cavitation. We shall show that the interfacial status captured by the MGFM can achieve "third-order accuracy" in the sense of comparing to the exact solution for any multi-fluid Riemann problem. Moreover, we shall find that the implicit ARPS based on a doubled shock structure is much stable and suitable for almost any initial conditions without restrictions in predicting the interfacial status, while a "natural" approach, which is also a "third-order" approximation, is proved to be less useful. It should be noted that the "accuracy" discussed in this paper means how accurate the boundary conditions are implicitly imposed at the material interface and how accurate the interface states are approximated by the GFM technique, which is in contrast with the accuracy of the numerical scheme or the errors between the exact solution and the numerical solution.

The paper is organized as follows. In Section 2 we introduce the Euler equations and equations of state (EOS) followed by a brief description of the level set equation. In Section 3 the solution structure of a multi-fluid Riemann problem is presented. In this section, the estimates about the interfacial status of the Riemann problem are derived and discussed. These estimates will serve as the basis for accuracy analysis of the MGFM. In Section 4, the multi-fluid Riemann problem is split into two pure fluid Riemann prob-

lems with one-sided ghost fluid defined, which are called GFM Riemann problems. The interfacial pressure and velocity provided by the two GFM Riemann problems in association with the MGFM are compared to the exact solution in order to analyze the accuracy of the MGFM. Then, we have some discussions on the prediction of the interfacial status in Section 5. The comparison between the "natural" approach and the implicit ARPS is shown in this section, and the "third-order accuracy" of the MGFM with the implicit ARPS is also illustrated by several numerical experiments. Finally, conclusions are drawn in Section 6.

2 Equations

2.1 The Euler equations

The one-dimensional Euler equations of an initial-value Riemann problem can be written as

$$\frac{\partial U}{\partial t}+\frac{\partial F(U)}{\partial x}=0,\quad U|_{t=0}=\begin{cases} U_l, & x<x_0,\\ U_r, & x>x_0,\end{cases} \tag{2.1}$$

for an inviscid, non-heat-conducting compressible flow, where $U=[\rho,\rho u,E]^T$, and $F(U)=[\rho u,\rho u^2+p,(E+p)u]^T$. Here ρ is the density, u is the velocity, p is the pressure, and E is the total energy per unit volume. The total energy is written as

$$E=\rho e+\frac{1}{2}\rho u^2, \tag{2.2}$$

where e is the internal energy per unit mass. U_l and U_r are two constant states separated by the material interface located at x_0. Hereafter, the subscripts "l" and "r" indicate the flow state on the left- and right-hand medium respectively.

2.2 Equations of state (EOS)

For closure of system (2.1), EOS is required. In the present work, our interest focuses on the compressible fluid media, such as gases and water. For gases the γ-law is used as

$$p=(\gamma_g-1)\rho e, \tag{2.3}$$

and for water the stiff gas EOS has the form

$$p=(\gamma_w-1)\rho e-\gamma_w B_w. \tag{2.4}$$

The EOS for the two fluids above can be expressed in the following consistent form as

$$p=(\gamma-1)\rho e-\gamma B, \tag{2.5}$$

where γ and B are different for different media. See Table 1 for the special cases of air and water. In the following, our accuracy analysis for the MGFM is based on EOS (2.5). The associated sound speed can then be expressed as $c=\sqrt{\gamma\overline{p}/\rho}$, where $\overline{p}=p+B$.

Table 1: Constant values γ and B for air and water.

Fluids	γ	B (Pa)
Air	1.4	0
Water	7.15	3.309×10^8

2.3 Level set equation

To track the moving material interface, the level set technique is employed. The zero level of the level set function ϕ marks the location of the interface, while the positive values correspond to one fluid and the negative values correspond to the other. The level set equation for one-dimensional flows can be written as

$$\frac{\partial\phi}{\partial t}+u\frac{\partial\phi}{\partial x}=0. \tag{2.6}$$

In general, $\phi(x,t)$ is initialized as the signed distance taken from the interface with reinitialization [17].

3 Solution structure and interface estimation

For a multi-fluid Riemann problem, where the fluids consist of gases or water, the structure of the solution is very similar to that for a pure gas Riemann problem [23], if the existence of vacuum or cavitation is excluded. The solution structure in general consists of four constant regions connected by one of the three centered Riemann waves: two nonlinear waves (shock wave and rarefaction wave) and a linear wave (contact discontinuity or material interface). The two nonlinear waves are separated by the linear wave, as depicted in Fig. 1(a).

Next, we establish some relationships between the exact interfacial status and the initial conditions. In each medium, there is only one Riemann wave, which is a nonlin-

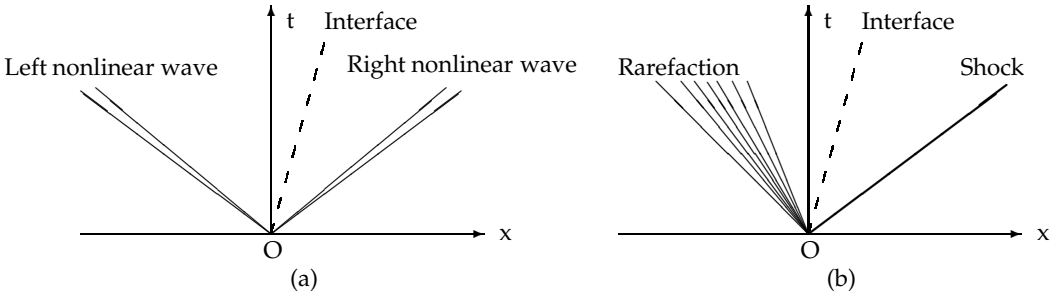

Figure 1: Structure of the solution of a Riemann problem for 1D Euler equations. (a) The general case in which two nonlinear Riemann waves are separated by the linear wave (interface). (b) A particular case in which the left wave is a rarefaction and the right wave is a shock.

ear wave. As shown in Fig. 1(b), if a rarefaction wave is generated in the left medium, via application of the Riemann invariant ($u+2c/(\gamma_l-1)=const$) and the isentropic law ($\overline{p}/\rho^{\gamma_l}=const$) through the rarefaction wave fan, we have following expression

$$u_l-u_I^e=\frac{2c_l}{\gamma_l-1}\left[\left(\frac{p_I^e+B_l}{\overline{p}_l}\right)^{\frac{\gamma_l-1}{2\gamma_l}}-1\right], \tag{3.1}$$

while if the left wave is a shock wave we obtain

$$u_l-u_I^e=\frac{1}{\rho_l c_l}\frac{p_I^e-p_l}{\sqrt{1+\frac{\gamma_l+1}{2\gamma_l}\left(\frac{p_I^e+B_l}{\overline{p}_l}-1\right)}}, \tag{3.2}$$

using the shock wave relationship. Here, the subscript "I" means interface location and the superscript "e" denotes exact value.

Similarly, for the right nonlinear wave we have

$$u_I^e-u_r=\frac{2c_r}{\gamma_r-1}\left[\left(\frac{p_I^e+B_r}{\overline{p}_r}\right)^{\frac{\gamma_r-1}{2\gamma_r}}-1\right], \tag{3.3}$$

$$u_I^e-u_r=\frac{1}{\rho_r c_r}\frac{p_I^e-p_r}{\sqrt{1+\frac{\gamma_r+1}{2\gamma_r}\left(\frac{p_I^e+B_r}{\overline{p}_r}-1\right)}}, \tag{3.4}$$

for the respective rarefaction wave and shock wave.

Then, considering the right parts of Eqs. (3.1)-(3.4) and using Taylor series expansion at $\overline{p}/\overline{p}_k$ around 1 (i.e. $|\overline{p}/\overline{p}_k-1|<1$), we can get the following relationships

$$\frac{2c_k}{\gamma_k-1}\left[\left(\frac{\overline{p}}{\overline{p}_k}\right)^{\frac{\gamma_k-1}{2\gamma_k}}-1\right]=\frac{c_k}{\gamma_k}\left(\frac{\overline{p}}{\overline{p}_k}-1\right)\left[1-\frac{\gamma_k+1}{4\gamma_k}\left(\frac{\overline{p}}{\overline{p}_k}-1\right)\right]+\mathcal{O}\left(\frac{\overline{p}}{\overline{p}_k}-1\right)^3, \tag{3.5}$$

$$\frac{1}{\rho_k c_k}\frac{p-p_k}{\sqrt{1+\frac{\gamma_k+1}{2\gamma_k}\left(\frac{\overline{p}}{\overline{p}_k}-1\right)}}=\frac{c_k}{\gamma_k}\left(\frac{\overline{p}}{\overline{p}_k}-1\right)\left[1-\frac{\gamma_k+1}{4\gamma_k}\left(\frac{\overline{p}}{\overline{p}_k}-1\right)\right]+\mathcal{O}\left(\frac{\overline{p}}{\overline{p}_k}-1\right)^3, \tag{3.6}$$

where $\overline{p}=p+B_k$, and the subscript "k" indicates "l" or "r". It is clearly found that the right parts in Eqs. (3.5) and (3.6) are exactly the same in form, but they are different for further higher-order Taylor expansion. According to (3.1)-(3.6) we have the following two expressions for the left and right nonlinear Riemann waves regardless of the types of these Riemann waves:

$$u_l-u_I^e=\frac{c_l}{\gamma_l}\left(\frac{p_I^e+B_l}{\overline{p}_l}-1\right)\left[1-\frac{\gamma_l+1}{4\gamma_l}\left(\frac{p_I^e+B_l}{\overline{p}_l}-1\right)\right]+\mathcal{O}\left(\frac{p_I^e+B_l}{\overline{p}_l}-1\right)^3, \tag{3.7}$$

$$u_I^e-u_r=\frac{c_r}{\gamma_r}\left(\frac{p_I^e+B_r}{\overline{p}_r}-1\right)\left[1-\frac{\gamma_r+1}{4\gamma_r}\left(\frac{p_I^e+B_r}{\overline{p}_r}-1\right)\right]+\mathcal{O}\left(\frac{p_I^e+B_r}{\overline{p}_r}-1\right)^3. \tag{3.8}$$

Utilizing (3.7) and (3.8) we can obtain the "third-order" approximation of interfacial pressure and velocity, as the following lemma states.

Lemma 3.1. *For the Riemann problem* (2.1)*, if the exact interfacial pressure* p_I^e *satisfies*

$$p_I^e < \min(2p_l+B_l, 2p_r+B_r), \tag{3.9}$$

then the pressure p_{INT} *and velocity* u_{INT} *are determined by the following system of quadratic equations*

$$\begin{cases} u_l-u_{INT}=\dfrac{1}{\rho_l c_l}(p_{INT}-p_l)\left[1-\dfrac{\gamma_l+1}{4\rho_l c_l^2}(p_{INT}-p_l)\right], \\ u_{INT}-u_r=\dfrac{1}{\rho_r c_r}(p_{INT}-p_r)\left[1-\dfrac{\gamma_r+1}{4\rho_r c_r^2}(p_{INT}-p_r)\right]. \end{cases} \tag{3.10}$$

Solving (3.10) *gives one branch of the solution:*

$$\begin{cases} u_{INT}=\dfrac{UU_{(1)}+UU_{(2)}+UU_{(3)}+UU_{(4)}+UU_{(5)}+UU_{(6)}}{4[(\gamma_r+1)\rho_l^2c_l^3+(\gamma_l+1)\rho_r^2c_r^3]^2}, \\ p_{INT}=\dfrac{\rho_l^2c_l^3[(\gamma_r+1)p_r+2\rho_r c_r^2]+\rho_r^2c_r^3[(\gamma_l+1)p_l+2\rho_l c_l^2]-\rho_l c_l\rho_r c_r\sqrt{PP}}{(\gamma_r+1)\rho_l^2c_l^3+(\gamma_l+1)\rho_r^2c_r^3}, \end{cases} \tag{3.11}$$

where

$$\begin{aligned} UU_{(1)}&=2(\gamma_l+1)(\gamma_r+1)\rho_l c_l\rho_r c_r(p_r-p_l)\left(2c_l c_r(\rho_l c_l+\rho_r c_r)-\sqrt{PP}\right), \\ UU_{(2)}&=4\rho_l c_l\rho_r c_r\left((\gamma_l+1)\rho_r c_r^2-(\gamma_r+1)\rho_l c_l^2\right)\left(2c_l c_r(\rho_l c_l+\rho_r c_r)-\sqrt{PP}\right), \\ UU_{(3)}&=-4(p_r-p_l)\left((\gamma_r+1)^2\rho_l^3c_l^5+(\gamma_l+1)^2\rho_r^3c_r^5\right), \\ UU_{(4)}&=-(\gamma_l+1)(\gamma_r+1)(p_r-p_l)^2\left((\gamma_l+1)\rho_r^2c_r^3-(\gamma_r+1)\rho_l^2c_l^3\right), \\ UU_{(5)}&=4(\gamma_l+1)(\gamma_r+1)\rho_l^2c_l^3\rho_r^2c_r^3(u_l+u_r), \\ UU_{(6)}&=4\left((\gamma_r+1)^2\rho_l^4c_l^6u_l+(\gamma_l+1)^2\rho_r^4c_r^6u_r\right), \end{aligned}$$

and

$$\begin{aligned} PP=c_l c_r\Big(&4(\gamma_r+1)\rho_l c_l^2(p_r-p_l)-4(\gamma_l+1)\rho_r c_r^2(p_r-p_l)-(\gamma_l+1)(\gamma_r+1)(p_r-p_l)^2 \\ &+4(\rho_l c_l+\rho_r c_r)^2c_l c_r+4(\gamma_r+1)\rho_l^2c_l^3(u_r-u_l)+4(\gamma_l+1)\rho_r^2c_r^3(u_r-u_l)\Big), \end{aligned}$$

which approximate the respective exact interfacial pressure p_I^e *and velocity* u_I^e *to the accuracy of* $\mathcal{O}\{\max[\,|(p_I^e+B_l)/\overline{p}_l-1|,|(p_I^e+B_r)/\overline{p}_r-1|]\}^3$ *regardless of the solution type.*

We should note that there are two solutions to (3.10), however, if we consider the simplest case where the flow states on both sides are exactly the same, namely $\rho_l=\rho_r$, $u_l=u_r$, $p_l=p_r$, $c_l=c_r$ and $\gamma_l=\gamma_r$, obviously the pressure solution $p_{\mathbb{NI}}$ should be $p_l(=p_r)$. Only the solution (3.11) is the correct choice. Furthermore, condition (3.9) implies that the higher-order terms in (3.7) and (3.8) are less than 1 (i.e. $|\overline{p}/\overline{p}_k-1|<1$). Lemma 3.1 is fundamental in analyzing the accuracy and error estimation of the MGFM in the next section.

4 Error estimation on MGFM

4.1 MGFM and ARPS

The GFM-based technique, when employed to solve the multi-fluid Riemann problem (2.1), requires essentially solving two separate pure medium Riemann problems (called GFM Riemann problems [8, 9]) in the respective media with associated one-sided ghost fluid in each time step. One is for the left fluid medium and the initial conditions are defined as

$$U|_{t=0}=\begin{cases} U_l, & x<x_0, \\ U_r^*, & x>x_0. \end{cases} \tag{4.1}$$

It solves from the grid node 1 on the left end to the ghost nodes. The other is in the right medium with the initial conditions of

$$U|_{t=0}=\begin{cases} U_l^*, & x<x_0, \\ U_r, & x>x_0, \end{cases} \tag{4.2}$$

and it solves from the ghost nodes to the end node on the right. Hereafter, "$*$" indicates the ghost fluid (status). In the modified GFM (MGFM) first presented in [8], the ghost fluid status U_r^* (U_l^*) is defined using the interfacial status, which is obtained by approximately solving a multi-medium Riemann problem along the normal direction of the interface. This is a salient feature of the MGFM and also a primary difference from the original GFM.

More concretely, there are two nonlinear characteristics intersecting at the interface: one stems from the left medium flow while the other originates from the right medium flow. They can be written in association with system (2.1) along the normal direction of the interface as

$$\frac{\mathrm{d}p_I}{\mathrm{d}t}+\rho_I^L c_I^L\frac{\mathrm{d}u_I}{\mathrm{d}t}=0, \quad \text{along } \frac{\mathrm{d}x}{\mathrm{d}t}=u_I+c_I^L, \tag{4.3a}$$

$$\frac{\mathrm{d}p_I}{\mathrm{d}t}-\rho_I^R c_I^R\frac{\mathrm{d}u_I}{\mathrm{d}t}=0, \quad \text{along } \frac{\mathrm{d}x}{\mathrm{d}t}=u_I-c_I^R, \tag{4.3b}$$

where the subscript "I" refers to the interface, and the superscript "L" and "R" denote the left side of the interface and the right side of the interface respectively. $\rho_I^L(\rho_I^R)$ and $c_I^L(c_I^R)$ are the density and sound speed on the left (right) side of the interface; p_I and u_I

represent the pressure and velocity at the interface. During the moment of a shock/jet impacting on the interface, pressure and velocity singularities are created at the interface, which means the pressure and velocity are not continuous across the interface. The above system, therefore, has to be specially solved ensuring the correct decomposition of these singularities. As such, an approximate Riemann problem solver (ARPS) based on a doubled shock structure [13] can be employed to solve for system and written as

$$\frac{p_I-p_{IL}}{W_{IL}}+(u_I-u_{IL})=0, \tag{4.4a}$$

$$\frac{p_I-p_{IR}}{W_{IR}}-(u_I-u_{IR})=0, \tag{4.4b}$$

where

$$W_{IL}=\rho_{IL}c_{IL}\sqrt{1+\frac{\gamma_l+1}{2\gamma_l}\left(\frac{p_I+B_l}{\overline{p}_{IL}}-1\right)},\quad W_{IR}=\rho_{IR}c_{IR}\sqrt{1+\frac{\gamma_r+1}{2\gamma_r}\left(\frac{p_I+B_r}{\overline{p}_{IR}}-1\right)}.$$

In practice, we firstly determine the states U_{IL} (i.e. ρ_{IL},u_{IL},p_{IL},c_{IL}) and U_{IR} (i.e. ρ_{IR},u_{IR}, p_{IR},c_{IR}) in (4.4). Assuming that the interface is located between node i and $i+1$ at time $t=t^n$, to compute the flow field at the next time step of $t=t^{n+1}$, we first obtain U_{IL} and U_{IR} via interpolation along the characteristic lines $\mathrm{d}x/\mathrm{d}t=u_I+c_I^L$ and $\mathrm{d}x/\mathrm{d}t=u_I-c_I^R$ tracing back from the interface into the respective Medium 1 and Medium 2. Alternatively, U_{IL} and U_{IR} can simply be taken as U_{i-1} and U_{i+2} respectively. Then, the interfacial status can be obtained by solving (4.4) using iterative method, as depicted briefly in Fig. 2(a).

Next, to define the ghost fluid status U_r^* in (4.1) for Medium 1, we use the predicted interfacial pressure and velocity as for the ghost fluid at the ghost node $i+1$. The ghost fluid pressure and velocity at the ghost node $i+2$ can be those for the real fluid (Medium 2) or predicted. The demonstration can be seen in Fig. 2(b). Finally, we employ isentropic fixing technique for eliminating the spurious overheating phenomenon [10] by fixing the real fluid density at node i and the ghost fluid density, with the predicted entropy s_I^L for Medium 1 at the interface. In more detail, because the status of ghost node $i+1$ is identified with the interfacial status, the entropy s_{i+1} is equivalent to the left interface value s_I^L. According to the isentropic law ($\overline{p}/\rho^\gamma=const$) we have

$$\rho_j=\rho_I^L\left(\frac{p_j+B_l}{p_I+B_l}\right)^{\frac{1}{\gamma_l}}, \tag{4.5}$$

where the subscript "j" represents node number. We just use this expression to fix the density values for node i, $i+2$ and $i+3$, as shown in Fig. 2(c). The ghost fluid status for Medium 2 is defined in a similar way except that the predicted entropy s_I^R for Medium 2 is used to assign the ghost fluid density. The new location of the interface is also obtained via solving the level set equation (2.6). Here we briefly summarize the general procedure of the MGFM, more details can be found in [8,9]:

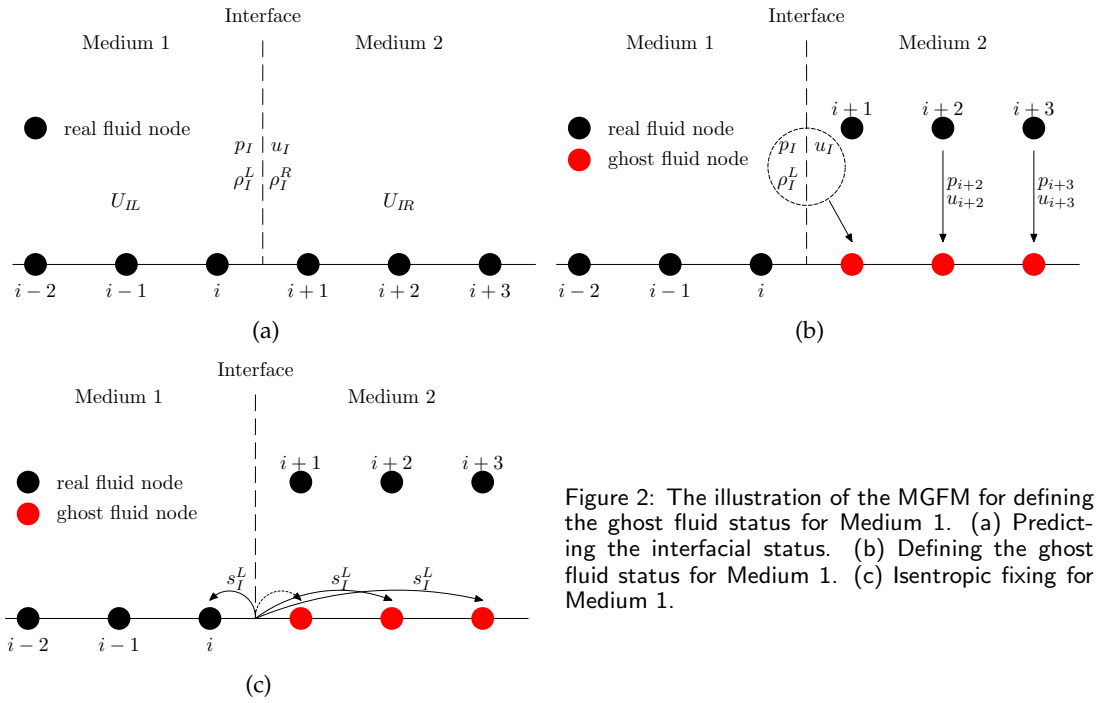

Figure 2: The illustration of the MGFM for defining the ghost fluid status for Medium 1. (a) Predicting the interfacial status. (b) Defining the ghost fluid status for Medium 1. (c) Isentropic fixing for Medium 1.

1. Advance the interface via solving the level set equation with reinitialization to the new time step, and get the new interface location.
2. Predict the interfacial status by constructing and solving the Riemann problem, and then use it to define the flow status in the ghost fluid.
3. Choose a suitable high-order single medium scheme to solve for each fluid medium. In that way the solution in all the media is advanced to the new time step.
4. Obtain the final solution over whole computation domain according to the new interface location, and then update the new time step size and proceed to the next time step.

4.2 Error estimation

For the MGFM applied to the Riemann problem (2.1), we use the predicted interfacial pressure and velocity to define the corresponding ghost fluid quantities, namely $p_r^*=p_I^M$, $u_r^*=u_I^M$, $p_l^*=p_I^M$ and $u_l^*=u_I^M$. Here p_I^M and u_I^M are calculated employing the ARPS:

$$\frac{p_I^M-p_l}{W_l}+(u_I^M-u_l)=0, \tag{4.6a}$$

$$\frac{p_I^M-p_r}{W_r}-(u_I^M-u_r)=0, \tag{4.6b}$$

where

$$W_l=\rho_l c_l\sqrt{1+\frac{\gamma_l+1}{2\gamma_l}\left(\frac{p_I^M+B_l}{\overline{p}_l}-1\right)},\quad W_r=\rho_r c_r\sqrt{1+\frac{\gamma_r+1}{2\gamma_r}\left(\frac{p_I^M+B_r}{\overline{p}_r}-1\right)}.$$

Before getting the error estimate for the MGFM, we need the following relationships applicable to ARPS (4.6):

(I) Relationships between the initial conditions and the predicted interfacial states

$$u_l-u_I^M=\frac{c_l}{\gamma_l}\left(\frac{p_I^M+B_l}{\overline{p}_l}-1\right)\left[1-\frac{\gamma_l+1}{4\gamma_l}\left(\frac{p_I^M+B_l}{\overline{p}_l}-1\right)\right]+\mathcal{O}\left(\frac{p_I^M+B_l}{\overline{p}_l}-1\right)^3, \tag{4.7a}$$

$$u_I^M-u_r=\frac{c_r}{\gamma_r}\left(\frac{p_I^M+B_r}{\overline{p}_r}-1\right)\left[1-\frac{\gamma_r+1}{4\gamma_r}\left(\frac{p_I^M+B_r}{\overline{p}_r}-1\right)\right]+\mathcal{O}\left(\frac{p_I^M+B_r}{\overline{p}_r}-1\right)^3; \tag{4.7b}$$

(II) Relationships between the predicted and the exact interfacial states

$$u_I^M-u_I^e=\mathcal{O}\left(\max\left[\left|\frac{p_I^e+B_l}{\overline{p}_l}-1\right|,\left|\frac{p_I^e+B_r}{\overline{p}_r}-1\right|\right]\right)^3, \tag{4.8a}$$

$$p_I^M-p_I^e=\mathcal{O}\left(\max\left[\left|\frac{p_I^e+B_l}{\overline{p}_l}-1\right|,\left|\frac{p_I^e+B_r}{\overline{p}_r}-1\right|\right]\right)^3. \tag{4.8b}$$

Because the ARPS employed is a doubled shock Riemann solver, p_I^M and u_I^M are identical to the exact interfacial states p_I^e and u_I^e for shock wave case, and are "third-order" approximation to the exact interfacial states for rarefaction wave case. (4.7) can be easily shown by applying (3.6) to ARPS (4.6). Obviously, they are similar to (3.7) and (3.8) in form. (4.8) can be derived by utilizing the two relationships (4.7) and Lemma 3.1. According to (4.7)-(4.8) we have following conclusions held for the MGFM with ARPS (4.6) when applied to the Riemann problem (2.1).

Theorem 4.1. *The MGFM is "third-order" accurate theoretically when applied to treat the interface for the original Riemann problem* (2.1) *regardless of the solution type. That is, the following error estimates are valid for the respective GFM Riemann problems* (4.1) *and* (4.2) *using the MGFM with ARPS* (4.6)*:*

$$u_I^{MA}-u_I^e=\mathcal{O}\left(\frac{p_I^e+B_l}{\overline{p}_l}-1\right)^3, \tag{4.9a}$$

$$p_I^{MA}-p_I^e=\mathcal{O}\left(\frac{p_I^e+B_l}{\overline{p}_l}-1\right)^3, \tag{4.9b}$$

$$u_I^{MB}-u_I^e=\mathcal{O}\left(\frac{p_I^e+B_r}{\overline{p}_r}-1\right)^3, \tag{4.10a}$$

$$p_I^{MB}-p_I^e=\mathcal{O}\left(\frac{p_I^e+B_r}{\overline{p}_r}-1\right)^3, \tag{4.10b}$$

where $u_I^{MA}(u_I^{MB})$ and $p_I^{MA}(p_I^{MB})$ are the exact interfacial velocity and pressure of the GFM Riemann problem (4.1) (*(4.2)*) *using the MGFM.*

Proof. In each fluid medium, there is only one nonlinear wave. If the nonlinear wave is a shock wave in the left (right) medium, $u_I^{MA}(u_I^{MB})$ and $p_I^{MA}(p_I^{MB})$ are virtually identical to the exact interfacial velocity u_I^e and pressure p_I^e, because ARPS (4.6) is just based on a doubled shock structure. In that case the error estimates (4.9)-(4.10) are definitely established.

In the following, we only need to consider the case where a rarefaction wave is generated in either medium. Assume that in the left medium there is a rarefaction wave. According to MGFM for the GFM Riemann problem (4.1), we have $p_r^*=p_I^M$, $u_r^*=u_I^M$, $\gamma_r^*=\gamma_l$ and $B_r^*=B_l$. Note that $p_I^e<p_l$ for the left rarefaction wave case, thus condition (3.9) in Lemma 3.1 is automatically satisfied. Then, by applying Lemma 3.1 to the GFM Riemann problem (4.1), we have $|(p_I^{MA}+B_l)/\overline{p}_l-1|<1$ and get

$$u_I^{MA}=\frac{UU_{(1)}^A+UU_{(2)}^A+UU_{(3)}^A+UU_{(4)}^A+UU_{(5)}^A+UU_{(6)}^A}{4(\gamma_l+1)^2(\rho_l{}^2c_l{}^3+\rho_r^{*2}c_r^{*3})^2}+\mathcal{O}\left(\frac{p_I^{MA}+B_l}{\overline{p}_l}-1\right)^3, \tag{4.11a}$$

$$p_I^{MA}=\frac{(\gamma_l+1)(\rho_l{}^2c_l{}^3p_I^M+\rho_r^{*2}c_r^{*2}p_l)+2\rho_lc_l{}^2\rho_r^*c_r^{*2}(\rho_lc_l+\rho_r^*c_r^*)-\rho_lc_l\rho_r^*c_r^*\sqrt{PP^A}}{(\gamma_l+1)(\rho_l{}^2c_l{}^3+\rho_r^{*2}c_r^{*3})}$$
$$+\mathcal{O}\left(\frac{p_I^{MA}+B_l}{\overline{p}_l}-1\right)^3, \tag{4.11b}$$

where

$$\begin{aligned}
UU_{(1)}^A&=2(\gamma_l+1)^2\rho_lc_l\rho_r^*c_r^*(p_I^M-p_l)\left(2c_lc_r^*(\rho_lc_l+\rho_r^*c_r^*)-\sqrt{PP^A}\right),\\
UU_{(2)}^A&=4(\gamma_l+1)\rho_lc_l\rho_r^*c_r^*(\rho_r^*c_r^{*2}-\rho_lc_l^2)\left(2c_lc_r^*(\rho_lc_l+\rho_r^*c_r^*)-\sqrt{PP^A}\right),\\
UU_{(3)}^A&=-4(\gamma_l+1)^2(p_I^M-p_l)(\rho_l^3c_l^5+\rho_r^{*3}c_r^{*5}),\\
UU_{(4)}^A&=-(\gamma_l+1)^3(p_I^M-p_l)^2(\rho_r^{*2}c_r^{*3}-\rho_l^2c_l^3),\\
UU_{(5)}^A&=4(\gamma_l+1)^2\rho_l^2c_l^3\rho_r^{*2}c_r^{*3}(u_l+u_I^M),\\
UU_{(6)}^A&=4(\gamma_l+1)^2(\rho_l^4c_l^6u_l+\rho_r^{*4}c_r^{*6}u_I^M),
\end{aligned}$$

and

$$\begin{aligned}
PP^A=&c_lc_r^*\Big(4(\gamma_l+1)(\rho_lc_l^2-\rho_r^*c_r^{*2})(p_I^M-p_l)-(\gamma_l+1)^2(p_I^M-p_l)^2\\
&+4(\rho_lc_l+\rho_r^*c_r^*)^2c_lc_r^*+4(\gamma_l+1)(\rho_l^2c_l^3+\rho_r^{*2}c_r^{*3})(u_I^M-u_l)\Big).
\end{aligned}$$

In order that the expressions (4.11a) and (4.11b) are meaningful, PP^A must not be negative. Substituting $u_I^M-u_l$ from (4.7a) into PP^A we obtain

$$PP^A=\frac{c_r^{*2}}{\rho_l^2c_l^2}\left[(\gamma_l+1)\rho_r^*c_r^*(p_l-p_I^M)+2\rho_lc_l^2(\rho_lc_l+\rho_r^*c_r^*)\right]^2+\mathcal{O}\left(\frac{p_I^M+B_l}{\overline{p}_l}-1\right)^3, \tag{4.12}$$

which indicates PP^A is positive and then the expressions of u_I^{MA} and p_I^{MA} are meaningful.

Next, we shall show the error estimates (4.9) are correct. Substituting (4.12) into (4.11) and after some manipulations, we find if

$$(\gamma_l+1)\rho_r^*c_r^*(p_l-p_I^M)+2\rho_l c_l^2(\rho_l c_l+\rho_r^* c_r^*)\geq 0, \tag{4.13}$$

then (4.11a) and (4.11b) can be simplified as

$$u_I^{MA}=u_I^M+\mathcal{O}\left(\frac{p_I^M+B_l}{\overline{p}_l}-1\right)^3+\mathcal{O}\left(\frac{p_I^{MA}+B_l}{\overline{p}_l}-1\right)^3, \tag{4.14a}$$

$$p_I^{MA}=p_I^M+\mathcal{O}\left(\frac{p_I^M+B_l}{\overline{p}_l}-1\right)^3+\mathcal{O}\left(\frac{p_I^{MA}+B_l}{\overline{p}_l}-1\right)^3. \tag{4.14b}$$

Using (4.8a) and (4.8b) we have

$$u_I^{MA}=u_I^e+\mathcal{O}\left(\frac{p_I^e+B_l}{\overline{p}_l}-1\right)^3+\mathcal{O}\left(\frac{p_I^{MA}+B_l}{\overline{p}_l}-1\right)^3, \tag{4.15a}$$

$$p_I^{MA}=p_I^e+\mathcal{O}\left(\frac{p_I^e+B_l}{\overline{p}_l}-1\right)^3+\mathcal{O}\left(\frac{p_I^{MA}+B_l}{\overline{p}_l}-1\right)^3. \tag{4.15b}$$

(4.15b) implies that

$$\mathcal{O}[(p_I^e+B_l)/\overline{p}_l-1]^3=\mathcal{O}[(p_I^{MA}+B_l)/\overline{p}_l-1]^3.$$

This directly leads to the satisfaction of error estimates (4.9), if (4.13) is held.

Then, we shall find out the condition for the establishment of (4.13). Set

$$f(\overline{p}_l)=(\gamma_l+1)\rho_r^*c_r^*(p_l-p_I^M)+2\rho_l c_l^2(\rho_l c_l+\rho_r^* c_r^*).$$

According to $p_l-p_I^M=\overline{p}_l-(p_I^M+B_l)$ and the sound speed relationship ($c_l^2=\gamma_l\overline{p}_l/\rho_l$, $c_r^{*2}=\gamma_l(p_I^M+B_l)/\rho_r^*$), we obtain

$$f(\overline{p}_l)=\frac{\gamma_l}{c_l c_r^*}\left(2\gamma_l c_r^*\overline{p}_l^2+(3\gamma_l+1)c_l(p_I^M+B_l)\overline{p}_l-(\gamma_l+1)c_l(p_I^M+B_l)^2\right).$$

It is easily found that there are two solutions to $f(\overline{p}_l)=0$ and the positive one is

$$\overline{p}_l^+=\frac{p_I^M+B_l}{4\gamma_l c_r^*}\left[\sqrt{(3\gamma_l+1)^2c_l^2+8\gamma_l(\gamma_l+1)c_l c_r^*}-(3\gamma_l+1)c_l\right]. \tag{4.16}$$

Applying basic inequality ($\sqrt{ab}<(a+b)/2$, if $a,b>0$ and $a\neq b$) gives

$$\overline{p}_l^+<\frac{\gamma_l+1}{3\gamma_l+1}(p_I^M+B_l), \tag{4.17}$$

which means if the condition

$$\overline{p}_l \geq \frac{\gamma_l+1}{3\gamma_l+1}(p_I^M+B_l) \quad \text{or} \quad p_I^M+B_l \leq \frac{3\gamma_l+1}{\gamma_l+1}\overline{p}_l \tag{4.18}$$

is satisfied, the value of $f(\overline{p}_l)$ will be positive. (4.18) implies that $p_I^M < 2p_l+B_l$ as $\gamma_l > 1$ physically. This makes (4.13) always true because for a rarefaction wave we have $p_I^e < p_l$ and p_I^M is a "third-order" approximation to p_I^e. Consequently, the error estimates (4.9) are held.

In a similar way, assuming that in the right medium there is a rarefaction wave, we can show the error estimates (4.10) are held for the GFM Riemann problem (4.2) when the MGFM is employed to treat the interface for the Riemann problem (2.1). Overall, whichever nonlinear wave is generated, the error estimates (4.9)-(4.10) are true. □

It should be pointed out that the error estimate is not expressed in the classical form of $\mathcal{O}(\Delta x)^d$ because the solution to Riemann problem (2.1) can be discontinuous in the vicinity of the interface. If the interface is in balance (that is the pressure and normal velocity are continuous across the interface), we have $p_l = p_I^e + \mathcal{O}(\Delta x)$ and the error expression returns to the classical form of $\mathcal{O}(\Delta x)^d$ and then the "order of accuracy" assumes the classical meaning.

It should be further noted that the error estimates in Theorem 4.1 are optimal, because as far as rarefaction is concerned, the solutions u_I^M and p_I^M to ARPS (4.6) approximate the exact interfacial velocity and pressure to "third-order accuracy", but they cannot achieve further higher-order accuracy. This can be shown by comparison of (3.5) and (3.6) and in combination with (4.7)-(4.8). Therefore, we cannot get further higher-order error estimates similar to (4.9)-(4.10) in Theorem 4.1.

To validate the above accuracy analysis of the MGFM with ARPS (4.6), we construct and solve a set of helium-air Riemann problems. The right initial states are fixed by $\rho_r = 1.0$, $u_r = 0.0$, $p_r = 100.0$. The left density and velocity are also fixed by $\rho_l = 1.0$, $u_l = 0.0$. We adjust the left pressure p_l to make $p_I^e/p_r - 1$ halved repeatedly. Once p_I^e is given, the left pressure p_l can be determined. Such a design is to testify conclusions (4.10) in Theorem 4.1. The nonlinear Riemann wave in the right side can be a rarefaction wave or a shock wave with the proper adjustment of p_I^e although its initial state is fixed. Tables 2 and 3 show the order of accuracy when the Riemann wave generated in the right medium is a rarefaction wave and a shock wave, respectively. The results show that the error estimates (4.10) are indeed valid from the numerical viewpoint. Similar method can be applied to testify the error estimates (4.9) in Theorem 4.1.

5 Discussions on the prediction of the interfacial status

To better understand the "third-order accuracy" of the MGFM with ARPS (4.6), we shall provide some discussions on the prediction of the interfacial status. The implicit ARPS

Table 2: The order of accuracy for the case of a rarefaction wave generated.

p_I^e/p_r-1	$\lvert u_I^{MB}-u_I^e\rvert$	order	$\lvert p_I^{MB}-p_I^e\rvert$	order
-0.5	2.4791E-03	–	1.6196E-02	–
-0.25	1.2284E-04	4.33	1.1359E-03	3.83
-0.125	8.4280E-06	3.87	8.8936E-05	3.67
-0.0625	7.2827E-07	3.53	8.1532E-06	3.45
-0.03125	7.3394E-08	3.31	8.4509E-07	3.27
-0.015625	8.1467E-09	3.17	9.5101E-08	3.15
-0.0078125	9.5634E-10	3.09	1.1240E-08	3.08
-0.00390625	1.1574E-10	3.05	1.3648E-09	3.04

Table 3: The order of accuracy for the case of a shock wave generated.

p_I^e/p_r-1	$\lvert u_I^{MB}-u_I^e\rvert$	order	$\lvert p_I^{MB}-p_I^e\rvert$	order
0.5	4.6441E-04	–	7.7267E-03	–
0.25	6.4156E-05	2.86	9.1744E-04	3.07
0.125	6.4536E-06	3.31	8.4431E-05	3.44
0.0625	5.2600E-07	3.62	6.5549E-06	3.69
0.03125	3.7897E-08	3.79	4.6038E-07	3.83
0.015625	2.5557E-09	3.89	3.0644E-08	3.91
0.0078125	1.6693E-10	3.94	1.9890E-09	3.95
0.00390625	1.0768E-11	3.95	1.2800E-10	3.96

will be compared with an explicit approach of also "third-order accuracy" and the applicability of these two methods will be analyzed in theory. In addition, several numerical examples will be given to further illustrate the advantage of ARPS (4.6) by comparing with an explicit approach of "second-order accuracy".

5.1 The "natural" approach versus the implicit ARPS

Someone would "naturally" consider utilizing $u_{\mathbb{INT}}$ and $p_{\mathbb{INT}}$ in Lemma 3.1 as the predicted interfacial status and then as the ghost fluid status, in that they also approximate the respective exact interfacial velocity u_I^e and pressure p_I^e to "third-order accuracy" theoretically, independent of the solution type. Furthermore, in this approach, it seems that the procedure for finding $u_{\mathbb{INT}}$ and $p_{\mathbb{INT}}$ is much easier to be implemented, for the solution can be directly derived from (3.11), while it appears more complex to find u_I^M and p_I^M if ARPS (4.6) is used, for the solution needs to be solved by iterative method. We call the former the "natural" approach. Numerical applications also affirm that the "natural" approach indeed provides the same accurate results as the ARPS does, if the "natural" approach is workable. Below is a gas-gas Riemann problem that the "natural" approach works. The initial conditions for this case are

$$\begin{cases} x<0.5: & (\gamma_l,\rho_l,u_l,p_l)=(5/3,2.0,0.0,3.0), \\ x>0.5: & (\gamma_r,\rho_r,u_r,p_r)=(1.4,1.0,0.0,1.0). \end{cases} \tag{5.1}$$

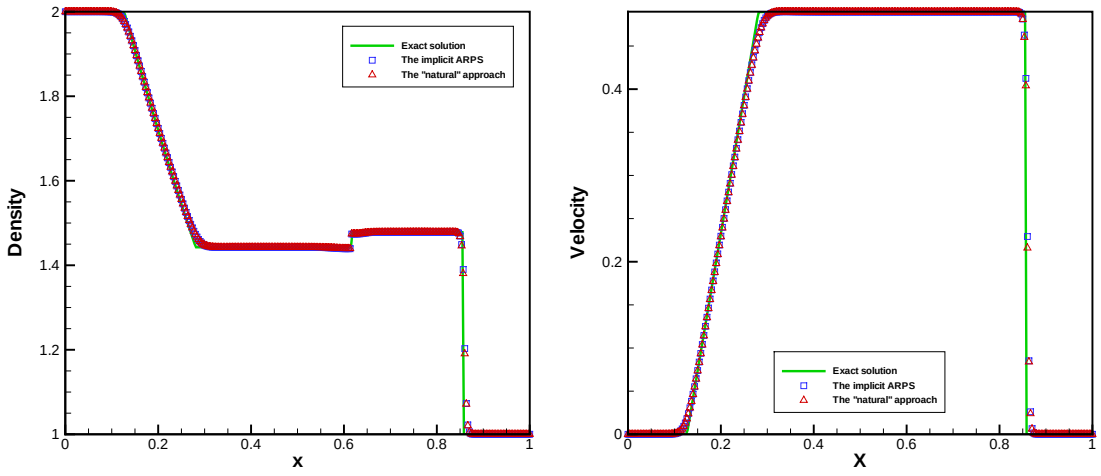

(a) (b)

Figure 3: Comparison of the "natural" approach with the implicit ARPS for predicting the interfacial status. (a) Density profile. (b) Velocity profile.

The computations are done using second-order HLL scheme with CFL$=$0.9 and 301 uniform mesh points in domain [0, 1]. Figs. 3(a) and 3(b) are the density and velocity profiles obtained after 150 time steps of computation. Results between the two methods look very similar, as was expected. Unfortunately, the existence conditions (in the physical meaning) of the solution via the "natural" approach are too strict to be satisfied usually in practice. As a matter of convenience, we also take the gas-gas Riemann problem as an example to illustrate the limitation of the "natural" approach in the following parts. Similar strategy can be employed in any multi-fluid Riemann problem.

In order to ensure the existence of the solution (3.11), PP must be positive or zero. Because the sound speed can be expressed as $c=\sqrt{\gamma p/\rho}$ for the gas-gas Riemann problem, PP can be expressed as

$$\begin{aligned}PP=&2(3\gamma_l+1)(3\gamma_r+1)p_lp_rc_lc_r+4\gamma_l^2p_l^2c_r^2+4\gamma_r^2p_r^2c_l^2-(5\gamma_l+1)(\gamma_r+1)p_l^2c_lc_r\\&-(5\gamma_r+1)(\gamma_l+1)p_r^2c_lc_r+4(\gamma_r+1)\gamma_l^2p_l^2c_r(u_r-u_l)+4(\gamma_l+1)\gamma_r^2p_r^2c_l(u_r-u_l).\end{aligned}\tag{5.2}$$

Note that $4\gamma_l^2p_l^2c_r^2+4\gamma_r^2p_r^2c_l^2\geq 8\gamma_l\gamma_rp_lp_rc_lc_r$. Moreover, we have

$$\begin{aligned}&4(\gamma_r+1)\gamma_l^2p_l^2c_r(u_r-u_l)+4(\gamma_l+1)\gamma_r^2p_r^2c_l(u_r-u_l)\\\geq&8\gamma_l\gamma_rp_lp_r(u_r-u_l)\sqrt{(\gamma_l+1)(\gamma_r+1)c_lc_r}\end{aligned}$$

for the situation where $u_r-u_l\geq 0$. By simple analysis we get

$$\frac{u_r-u_l}{\sqrt{c_lc_r}}\geq\max\left[0,\frac{(5\gamma_l+1)(\gamma_r+1)\frac{p_l}{p_r}+(5\gamma_r+1)(\gamma_l+1)\frac{p_r}{p_l}-2(13\gamma_l\gamma_r+3\gamma_l+3\gamma_r+1)}{8\gamma_l\gamma_r\sqrt{(\gamma_l+1)(\gamma_r+1)}}\right]\tag{5.3}$$

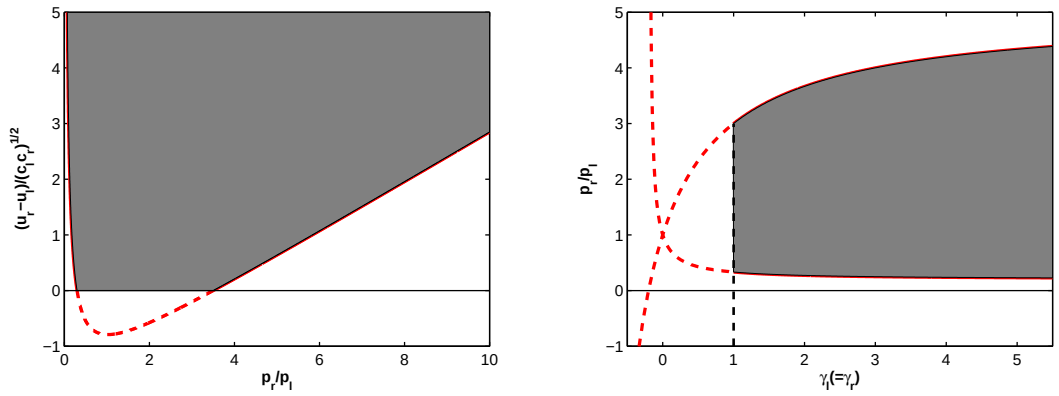

(a) (b)

Figure 4: Regions of inequality (5.3) are shown by shaded area. (a) The left gas is helium ($\gamma_l=5/3$) and the right gas is air ($\gamma_r=1.4$). (b) Both the velocities are identical ($u_l=u_r$).

as a sufficient condition of $PP\geq 0$. Fig. 4 illustrates the regions (dark zone) of inequality (5.3) under two specific conditions. In Fig. 4(a) the values of γ_l and γ_r are fixed. For example, the left and right gases are helium and air respectively. The abscissa indicates the initial pressure ratio and the ordinate indicates $(u_r-u_l)/\sqrt{c_l c_r}$. Clearly, the initial pressure ratio should be "appropriate"—not too large or too small, unless the value of $(u_r-u_l)/\sqrt{c_l c_r}$ is huge. In fact, condition (5.3) physically only includes weak shock wave or weak rarefaction wave cases and some strong doubled rarefaction waves cases. For further illustration of the limitation of the "natural" approach, we consider another simple problem where $u_r=u_l$, and then (5.3) reduces to

$$\frac{\gamma_r+1}{5\gamma_r+1}\leq\frac{p_r}{p_l}\leq\frac{5\gamma_l+1}{\gamma_l+1}. \tag{5.4}$$

This means the application range of the "natural" approach is limited to $p_r/p_l\in(1/5,5)$ due to $\gamma>1$ physically. See Fig. 4(b) where γ_l and γ_r are the same for simplicity. This also can be regarded as a simple shock tube problem. The abscissa indicates the ratio of specific heat and the ordinate indicates the initial pressure ratio. Any fixed value of abscissa results in a feasible range for the initial pressure ratio p_r/p_l and with the increase of abscissa the range does not change too much. This indicates that the "natural" approach when $u_r=u_l$ is only applicable for weak shock wave or weak rarefaction wave whatever kinds of gases are chosen. As for another situation, $u_r-u_l<0$, because the terms $4(\gamma_r+1)\gamma_l^2p_l^2c_r(u_r-u_l)$ and $4(\gamma_l+1)\gamma_r^2p_r^2c_l(u_r-u_l)$ in (5.2) are both negative, the application range of the "natural" approach is even more restricted. Even a slightly larger value of u_l-u_r will result in the failure of this approach. Various numerical experiments can also demonstrate our analysis. For the initial data (5.1), if all the conditions remain unaltered except that $p_l=3.0$ is replaced by $p_l=4.0$, or $u_l=0.0$ is replaced by $u_l=0.3$,

the "natural" approach does not work. In summary, the application conditions of this approach is very limited.

Another point that should be noted is that $p_{\mathbb{NT}}$ must always be positive. This requires

$$u_r-u_l<\frac{(5\gamma_l+1)c_l}{4\gamma_l^2}+\frac{(5\gamma_r+1)c_r}{4\gamma_r^2} \tag{5.5}$$

according to the expression of pressure in Lemma 3.1 for the "natural" approach. Any initial states U_l and U_r, which satisfy the condition (5.5), also satisfy the pressure physical positivity condition [23]

$$u_r-u_l<\frac{2c_l}{\gamma_l-1}+\frac{2c_r}{\gamma_r-1}, \tag{5.6}$$

so vacuum will not be created. Nevertheless, there may be such a situation of

$$\frac{(5\gamma_l+1)c_l}{4\gamma_l^2}+\frac{(5\gamma_r+1)c_r}{4\gamma_r^2}\leq u_r-u_l<\frac{2c_l}{\gamma_l-1}+\frac{2c_r}{\gamma_r-1}. \tag{5.7}$$

For this case, spurious vacuum will take place and then the "natural" approach is also inapplicable.

As far as ARPS (4.6) is concerned, we need to keep the terms $1+(\gamma_k+1)[(p_I^M+B_k)/\overline{p}_k-1]/(2\gamma_k)$ $(k=l,r)$ and the pressure solution p_I^M greater than zero. A note of caution is in order: if p_I^M remains positive, the terms mentioned above will definitely be greater than zero. Similar way for a positive solution for pressure p_I^M gives the following condition

$$u_r-u_l<\frac{c_l}{\gamma_l}\sqrt{\frac{2\gamma_l}{\gamma_l-1}}+\frac{c_r}{\gamma_r}\sqrt{\frac{2\gamma_r}{\gamma_r-1}}. \tag{5.8}$$

Likewise, there is a possibility that the initial states U_l and U_r might satisfy

$$\frac{c_l}{\gamma_l}\sqrt{\frac{2\gamma_l}{\gamma_l-1}}+\frac{c_r}{\gamma_r}\sqrt{\frac{2\gamma_r}{\gamma_r-1}}\leq u_r-u_l<\frac{2c_l}{\gamma_l-1}+\frac{2c_r}{\gamma_r-1}, \tag{5.9}$$

which will actually lead to the presence of two extremely strong rarefaction waves (close to the vacuum). Only for that case ARPS (4.6) cannot give the ideal result. However, the range of spurious vacuum condition (5.9) is much narrower than that of (5.7), which means the ARPS has a wider range of application than the "natural" approach, even under such extreme conditions. To avoid spurious vacuum, a doubled rarefaction Riemann solver is usually employed instead in the situation consisting of two strong rarefaction waves.

In conclusion, the solutions u_I^M and p_I^M to (4.6) are always meaningful except for the presence of extremely strong doubled rarefaction, unlike the solutions $u_{\mathbb{NT}}$ and $p_{\mathbb{NT}}$ via the "natural" approach, which are generally not applicable for slightly stronger shock wave cases and strong doubled rarefaction waves cases. Although $u_{\mathbb{NT}}$ and $p_{\mathbb{NT}}$ in Lemma 3.1 also approximate the respective exact interfacial velocity u_I^e and pressure p_I^e to "third-order accuracy", yet this approach is practically less useful.

5.2 A "second-order" method versus the implicit ARPS

According to (3.7) and (3.8) we can also obtain a "second-order" approximation of interfacial pressure and velocity, which is expressed as

$$\begin{cases} u_l - u_{\mathbb{INT}} = \dfrac{1}{\rho_l c_l}(p_{\mathbb{INT}} - p_l), \\ u_{\mathbb{INT}} - u_r = \dfrac{1}{\rho_r c_r}(p_{\mathbb{INT}} - p_r), \end{cases} \quad \text{or} \quad \begin{cases} u_{\mathbb{INT}} = \dfrac{\rho_l c_l u_l + \rho_r c_r u_r + p_l - p_r}{\rho_l c_l + \rho_r c_r}, \\ p_{\mathbb{INT}} = \dfrac{\rho_l c_l \rho_r c_r (u_l - u_r) + \rho_r c_r p_l + \rho_l c_l p_r}{\rho_l c_l + \rho_r c_r}. \end{cases} \tag{5.10}$$

The "second-order" method can also be utilized for predicting interfacial status. It is worth noting that this method has a wider range of application than the "natural" approach. The only restriction is the pressure solution $p_{\mathbb{INT}}$ should be positive. This requires

$$u_r - u_l < \frac{p_l}{\rho_l c_l} + \frac{p_r}{\rho_r c_r}. \tag{5.11}$$

In the following parts, some gas-water Riemann problems will be presented to test for both the "second-order" method and the implicit ARPS. All the computations are done using second-order HLL scheme with CFL$=0.9$ and 301 uniform mesh points in domain $[0,1]$. All the parameters are made non-dimensional and all the numerical results are obtained after 100 time steps of computation. We shall find that ARPS (4.6) can provide relatively excellent numerical results for all the cases below. As for the "second-order" method, it may produce some inaccurate solutions (Case 1-3), or even may not work (Case 4).

Case 1: The initial conditions are

$$\begin{cases} x < 0.5: & (\gamma_l, \rho_l, u_l, p_l) = (1.4, 0.6, -100.0, 10000.0), \\ x > 0.5: & (\gamma_r, \rho_r, u_r, p_r) = (7.15, 1.0, 0.0, 1.0). \end{cases} \tag{5.12}$$

This is a gas-water problem where a left rarefaction wave and a right shock wave are generated in respective media. Figs. 5(a), 5(b) and 5(c) are the density, velocity and pressure profiles obtained by the implicit ARPS and the explicit "second-order" method. For the explicit "second-order" method, there is distinctly visible overshoot found on the left side of the interface in the density profile. In addition, as observed at the tail of the left rarefaction, the result by this method has a minor hump in the velocity profile and a minor trough in the pressure profile. However, for the implicit ARPS, all the nonphysical phenomena disappear, and the location of the right shock front is predicted a little more accurately than the explicit "second-order" method.

Case 2: The initial conditions are

$$\begin{cases} x < 0.5: & (\gamma_l, \rho_l, u_l, p_l) = (1.4, 0.1, 50.0, 100.0), \\ x > 0.5: & (\gamma_r, \rho_r, u_r, p_r) = (7.15, 1.038, 20.0, 1000.0). \end{cases} \tag{5.13}$$

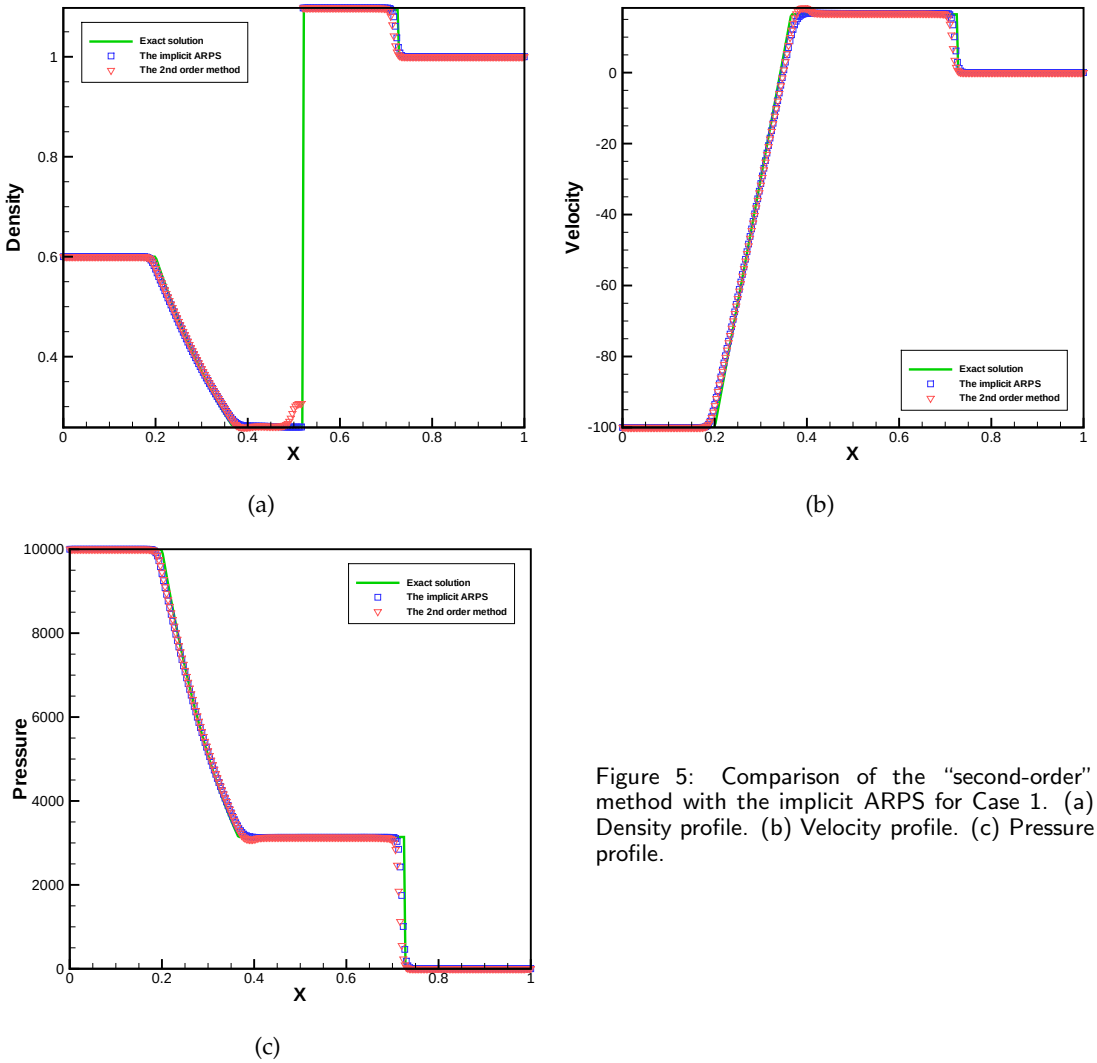

Figure 5: Comparison of the "second-order" method with the implicit ARPS for Case 1. (a) Density profile. (b) Velocity profile. (c) Pressure profile.

This is a gas-water problem where a left shock wave and a right rarefaction wave are generated in respective media. Figs. 6(a), 6(b) and 6(c) are the density, velocity and pressure profiles obtained by the implicit ARPS and the explicit "second-order" method. If the explicit "second-order" method is used, a large trough appears near the tail of the rarefaction in the pressure profile, while the implicit ARPS provides a reasonably correct result in comparison.

Case 3: The initial conditions are

$$\begin{cases} x<0.5: & (\gamma_l,\rho_l,u_l,p_l)=(1.4,0.1,200.0,500.0), \\ x>0.5: & (\gamma_r,\rho_r,u_r,p_r)=(7.15,1.0,0.0,1.0). \end{cases} \tag{5.14}$$

This is a gas-water problem where a left shock wave and a right shock wave are gener-

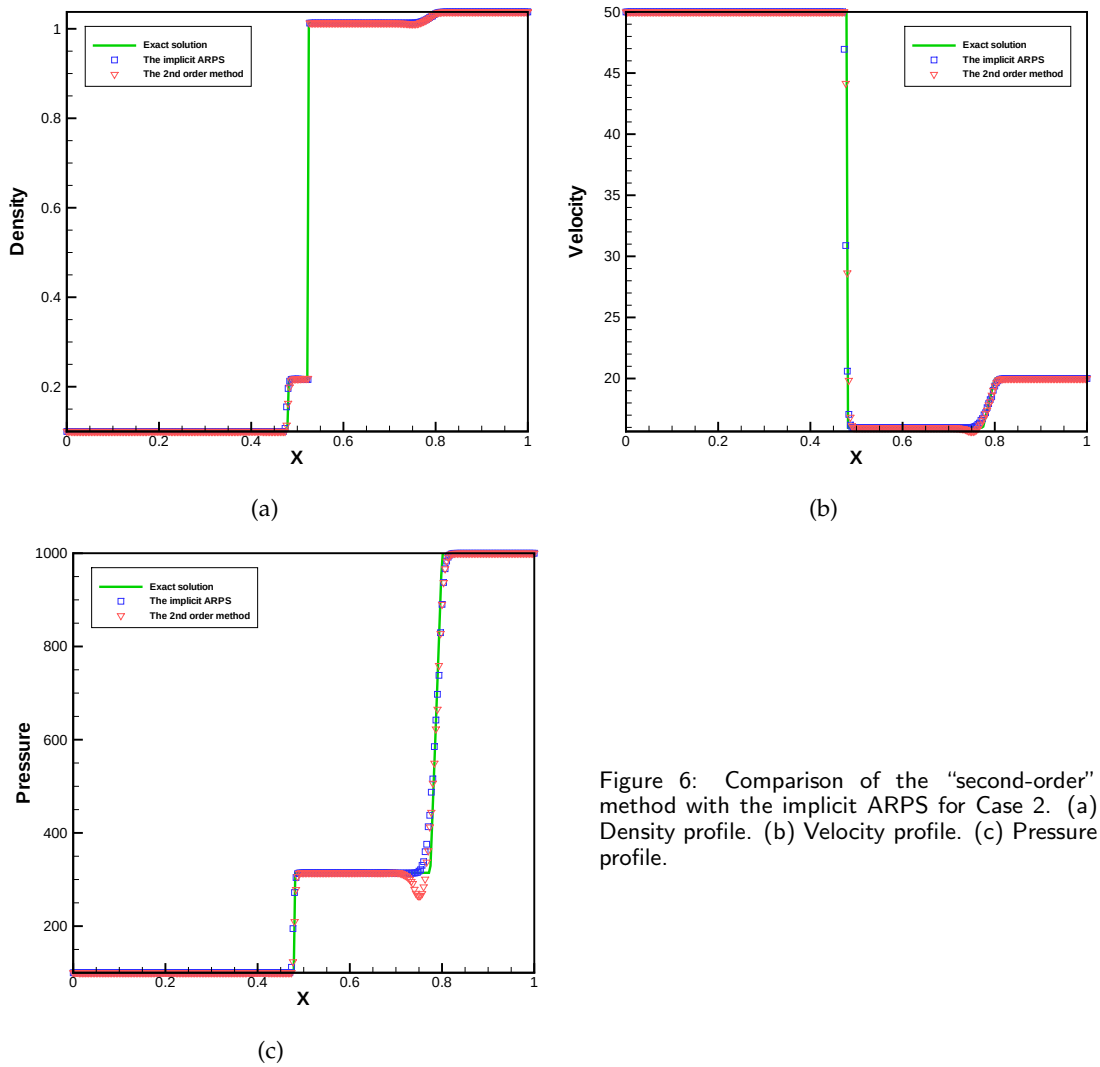

Figure 6: Comparison of the "second-order" method with the implicit ARPS for Case 2. (a) Density profile. (b) Velocity profile. (c) Pressure profile.

ated in respective media. Figs. 7(a), 7(b) and 7(c) are the density, velocity and pressure profiles obtained by the implicit ARPS and the explicit "second-order" method. For the "second-order" method, the locations of both the interface and the left shock front are captured accurately, but there is a little discrepancy at the location of the right shock front. Comparatively speaking, the results by the implicit ARPS concur well with the exact solution.

Case 4: The initial conditions are

$$\begin{cases} x<0.5: & (\gamma_l,\rho_l,u_l,p_l)=(1.4,0.2,-100.0,1000.0), \\ x>0.5: & (\gamma_r,\rho_r,u_r,p_r)=(7.15,1.202,0.0,9000.0). \end{cases} \tag{5.15}$$

This is a gas-water problem where a left rarefaction wave and a right rarefaction wave

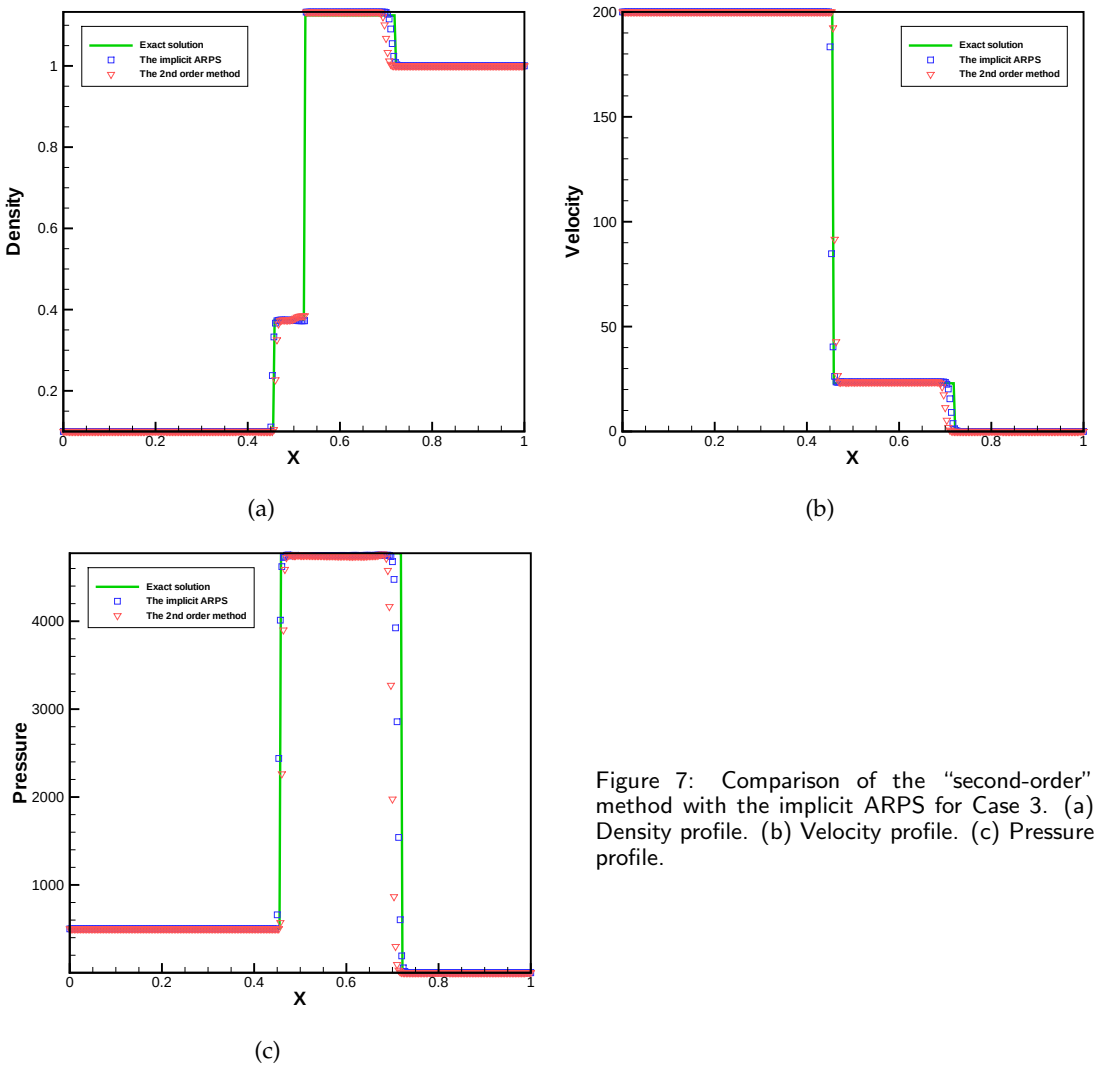

Figure 7: Comparison of the "second-order" method with the implicit ARPS for Case 3. (a) Density profile. (b) Velocity profile. (c) Pressure profile.

are generated in respective media. The initial conditions violate condition (5.11), so the explicit "second-order" method is not suited to this case. Nevertheless, we can still use the implicit ARPS to predict the interfacial states because the initial conditions do not violate condition (5.8). Figs. 8(a), 8(b) and 8(c) show that the density, velocity and pressure obtained by the implicit ARPS agree well with the theoretical results.

6 Conclusions

In this paper, a further analysis has been carried out rigorously for the MGFM when applied to any multi-fluid Riemann problem constituted with a stiffened gas EOS. Using

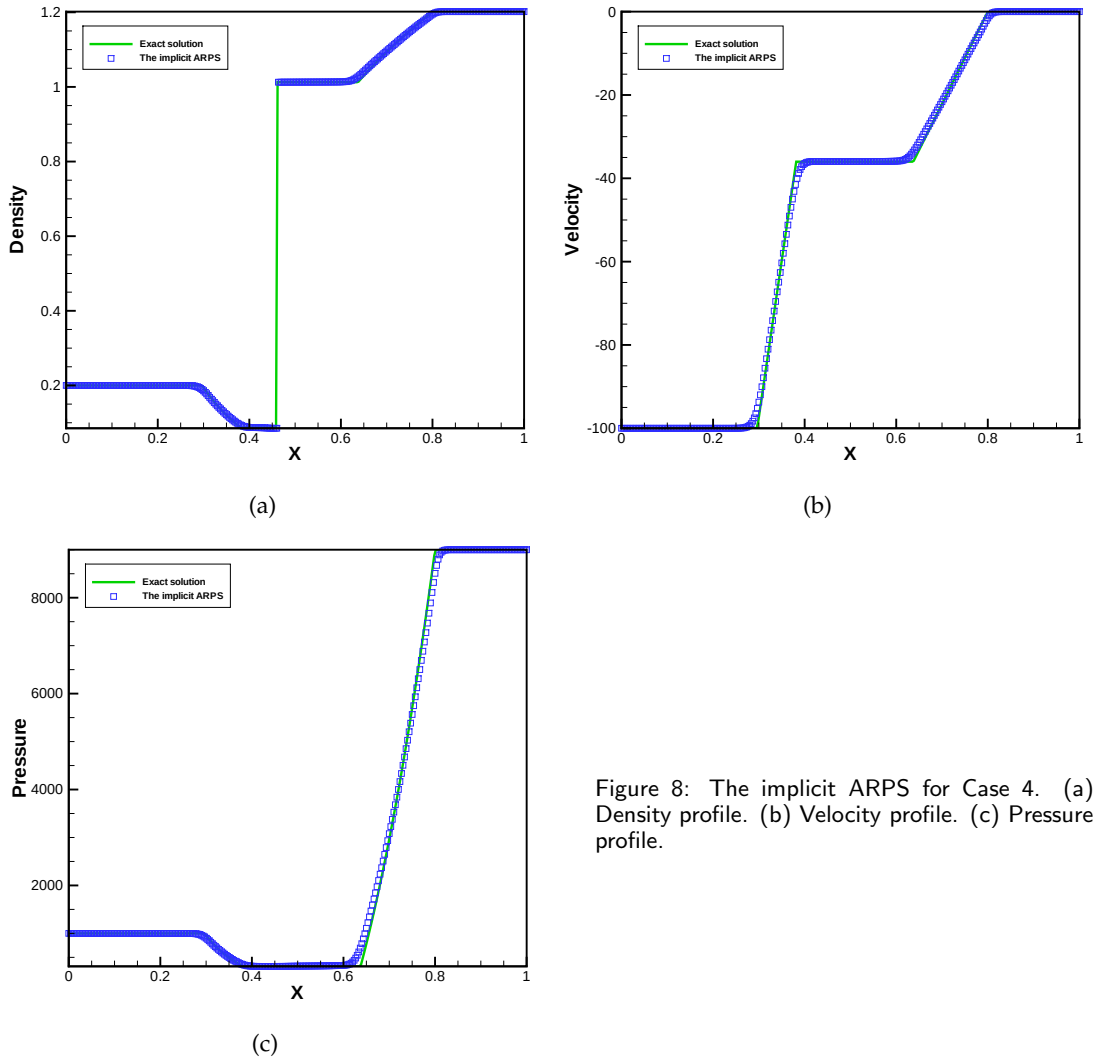

Figure 8: The implicit ARPS for Case 4. (a) Density profile. (b) Velocity profile. (c) Pressure profile.

the properties of the MGFM and the ARPS in the process of estimating the errors associated in determination of the interfacial status, we found that for any multi-fluid Riemann problem, the interfacial status captured by the MGFM can approximate the exact solution to "third-order accuracy", regardless of the solution type. Furthermore, through the discussion on choice of the predicted interfacial status, we recommended employing the implicit ARPS based on a doubled shock structure, which is suited to almost any initial conditions. In contrast, the "natural" approach of "third-order accuracy" is severely restricted and less useful, and another "second-order" method is not so accurate as the implicit ARPS. Of course, the current analytical skill is generally effective for fluid with stiffened gas EOS. The error estimation of the MGFM with a more general EOS will be studied and analyzed in the future work with a more advanced analytical skill.

Acknowledgments

The authors would like to thank the referees for valuable comments and suggestions. This work is supported under the National Natural Science Foundation of China (No. 10871018) and the funding of National Key Lab of Explosion Science and Technology (No. KFJJ08-7).

References

[1] A. Harten, High resolution schemes for hyperbolic conservation laws, J. Comput. Phys., 49 (1983), 357-393.
[2] A. Harten, On a class of high resolution total-variation-stable finite-difference schemes, SIAM J. Numer. Anal., 21 (1984), 1-23.
[3] A. Harten and S. Osher, Uniformly high-order accurate nonoscillatory schemes I, SIAM J. Numer. Anal., 24 (1987), 279-309.
[4] A. Harten, B. Engquist, S. Osher and S. R. Chakravarthy, Uniformly high-order accurate essentially nonoscillatory schemes III, J. Comput. Phys., 71 (1987), 231-303.
[5] C. W. Shu and S. Osher, Efficient implementation of essentially nonoscillatory shockcapturing schemes, J. Comput. Phys., 77 (1988), 439-471.
[6] R. Saurel and R. Abgrall, A multiphase Godunov method for compressible multifluid and multiphase flows, J. Comput. Phys., 150 (1999), 425-467.
[7] R. Abgrall and S. Karni, Compressible multifluid flows, J. Comput. Phys., 169 (2001), 594-623.
[8] T. G. Liu, B. C. Khoo and K. S. Yeo, Ghost fluid method for strong shock impacting on material interface, J. Comput. Phys., 190 (2003), 651-681.
[9] T. G. Liu, B. C. Khoo and C. W. Wang, The ghost fluid method for compressible gas-water simulation, J. Comput. Phys., 204 (2005), 193-221.
[10] R. P. Fedkiw, A. Marquina and B. Merriman, An isobaric fix for the overheating problem in multimaterial compressible flows, J. Comput. Phys., 148 (1999), 545-578.
[11] R. P. Fedkiw, T. Aslam, B. Merriman and S. Osher, A non-oscillatory Eulerian approach to interfaces in multimaterial flows (the ghost fluid method), J. Comput. Phys., 152 (1999), 457-492.
[12] R. P. Fedkiw, Coupling an Eulerian fluid calculation to a Lagrangian solid calculation with the ghost fluid method, J. Comput. Phys., 175 (2002), 200-224.
[13] T. G. Liu, B. C. Khoo and K. S. Yeo, The simulation of compressible multi-medium flow. Part I: A new methodology with test applications to 1D gas-gas and gas-water cases, Comput. Fluids, 30 (2001), 291-314.
[14] T. G. Liu, B. C. Khoo and K. S. Yeo, The simulation of compressible multi-medium flow. Part II: Applications to 2D underwater shock refraction, Comput. Fluids, 30 (2001), 315-337.
[15] E. H. van Brummelen and B. Koren, A pressure-invariant conservative Godunov-type method for barotropic two-fluid flows, J. Comput. Phys., 185 (2003), 289-308.
[16] R. R. Nourgaliev, T. N. Dinh and T. G. Theofanous, Adaptive characteristics-based matching for compressible multifluid dynamics, J. Comput. Phys., 213 (2006), 500-529.
[17] M. Sussman, P. Smereka and S. Osher, A level set approach for computing solutions to incompressible two-phase flow, J. Comput. Phys., 114 (1994), 146-159.

[18] T. G. Liu and B. C. Khoo, The accuracy of the modified ghost fluid method for gas-gas Riemann problem, Appl. Numer. Math., 57 (2007), 721-733.
[19] C. W. Wang, T. G. Liu and B. C. Khoo, A real-ghost fluid method for the simulation of multi-medium compressible flow, SIAM J. Sci. Comput., 28 (2006), 278-302.
[20] J. X. Qiu, T. G. Liu and B. C. Khoo, Simulations of compressible two-medium flow by Runge-Kutta discontinuous Galerkin methods with the ghost fluid method, Commun. Comput. Phys., 3 (2008), 479-504.
[21] T. G. Liu, W. F. Xie and B. C. Khoo, The modified ghost fluid method for coupling of fluid and structure constituted with hydro-elasto-plastic equation of state, SIAM J. Sci. Comput., 30 (2008), 1105-1130.
[22] T. G. Liu, B. C. Khoo and W. F. Xie, The modified ghost fluid method as applied to extreme fluid-structure interaction in the presence of cavitation, Commun. Comput. Phys., 1 (2006), 898-919.
[23] E. F. Toro, Riemann Solvers and Numerical Methods for Fluid Dynamics, Springer-Verlag Berlin Heidelbert, 1999.